Lawrence Berkeley National Laboratory

Title
Local-probe studies of degradation of composite LiNi0.8Co 0.15Al0.05O2 cathodes in high-power lithium-ion cells

Permalink
https://escholarship.org/uc/item/6zx934cc

Authors
Kostecki, Robert
McLarnon, Frank

Publication Date
2004-06-01

Local-Probe Studies of Degradation of Composite $LiNi_{0.8}Co_{0.15}Al_{0.05}O_2$ Cathodes in High-Power Lithium-Ion Cells

Robert Kostecki[*z] and Frank McLarnon[**]

Environmental Energy Technologies Division, Lawrence Berkeley National Laboratory,

University of California, Berkeley, California 94720, USA

ABSTRACT

High-power Li-ion cells that were tested at elevated temperatures showed a significant impedance rise, which was associated primarily with the $LiNi_{0.8}Co_{0.15}Al_{0.05}O_2$ cathode. Raman microscopy mapping provided evidence that the surface composition ratio between $LiNi_{0.8}Co_{0.15}Al_{0.05}O_2$ and carbon in the composite cathode increases upon cell aging and cycling. Current-sensing atomic force microscopy imaging of single grains of pristine $LiNi_{0.8}Co_{0.15}Al_{0.05}O_2$ powder revealed poor residual electronic contact between sub-micron primary particles within $LiNi_{0.8}Co_{0.15}Al_{0.05}O_2$ agglomerates. Carbon retreat or rearrangement that occurs during cell testing allows residual inter-particle resistance to dominate cathode interfacial charge-transfer impedance and accounts for the observed cell power and capacity loss.

Key words: Li-ion battery, cathode, carbon retreat, conductivity, micro-Raman, AFM

[*] Electrochemical Society Active Member
[z] r_kostecki@lbl.gov
[**] Electrochemical Society Fellow

INTRODUCTION

A primary goal of the U.S. Department of Energy's Advanced Technology Development (ATD) Program is the development of high-power Li-ion batteries for hybrid electric vehicle applications [1]. Diagnostic evaluations of Li-ion cells that were aged and/or cycled under various conditions were carried out to determine the mechanisms responsible for the cell power loss that accompanies life tests at elevated temperatures [2]. Impedance measurements of the cell components indicated that the $LiNi_{0.8}Co_{0.15}Al_{0.05}O_2$ cathode is primarily responsible for the observed cell power loss at elevated temperatures, similar to the $LiNi_{0.8}Co_{0.2}O_2$ cathode that was studied in our previous work [3]. Possible causes of the increase in cathode impedance include the formation of an electronic and/or ionic barrier at the cathode surface [1,4]. **However, the observation that, in these cells, power fade is always accompanied by the loss of discharge capacity is a somewhat general conclusion for several types of cathodes. The mechanism of power and capacity loss in the ATD high-power Li-ion cells may involve specific detrimental processes, which also occur in other Li-ion systems.**

The *in-situ* application of local probe techniques to characterize physico-chemical properties of the electrode-electrolyte interface, which is documented in a large number of published studies, not only provides unique insight into the mechanisms of electrochemical processes but also has stimulated the recent emergence of electrochemical nanotechnology.

Rey at al. [5] first demonstrated the successful application of confocal Raman micro-spectroscopy for *in-situ* characterization of a lithium battery that consisted of a Li metal anode, $P(EO)_{20}LiN(SO_2CF_3)_2$ polymer electrolyte, and a V_2O_5 cathode. An innovative application of Raman micro-spectroscopy was presented in studies by Panitz and Novák [6,7,8,9], who used Raman surface mapping to generate local surface composition images of 30x35 μm areas (at 2 μm lateral resolution) of $LiCoO_2$ positive and carbon negative electrodes from commercial lithium-ion batteries. The extraordinary potential of *in-situ* Raman micro-spectroscopy to study dynamic aspects of Li^+ intercalation-deintercalation process was illustrated by the work of Luo et al. [10,11], who collected good-quality, time-resolved Raman spectra from a single isolated micrometer-size particle of $LiMn_2O_4$ embedded in Au foil substrate and single graphite

particles embedded in thermally annealed Ni foils in nonaqueous electrolytes as a function of applied potential. Kostecki and McLarnon [12] investigated the microstructural stability of graphite anodes in Li-ion cells by Raman micro-spectroscopy imaging of the integrated intensity ratio of the D/G bands of carbon on 40 x 60 μm electrode surface areas, as well as the electrode cross-section, at 0.7 μm resolution.

X-ray diffraction spectroscopy measurements failed to detect noticeable changes in the bulk structure of tested ATD Program $LiNi_{0.8}Co_{0.15}Al_{0.05}O_2$ cathodes [1]. In the present study, we investigate detailed cathode surface processes, which accompanied cell storage and/or cycling. We demonstrate that of current-sensing AFM and Raman microscopy can provide unique information on complex surface phenomena, which are likely responsible for the composite cathode capacity fade and impedance increase.

EXPERIMENTAL

High-power Li-ion cells with a $LiNi_{0.8}Co_{0.15}Al_{0.05}O_2$ cathode, a synthetic graphite anode, 1.2 M $LiPF_6$ + ethylene carbonate + ethyl-methyl carbonate (EC/EMC) electrolyte, and a Celgard® 2300 separator, were manufactured, aged, cycled, and/or abused and then characterized under the ATD Program [1]. We compared a fresh cathode with cathodes taken from cells that were aged or cycled at elevated temperatures for up to 68 weeks, losing up to 52% of their initial power and 24% of their initial capacity.

All cathodes were soaked in dimethyl carbonate (DMC) for 30 minutes after removal from Li-ion cells inside an argon-filled glove box. This procedure removed electrolyte salt from the electrode to prevent its reaction with air and moisture. An integrated Raman microscope system "Labram" made by ISA Groupe Horiba was used to analyze and map the cathode surface structure and composition. The excitation source was an internal He-Ne (632 nm) 10 mW laser. The power of the laser beam was adjusted to 0.1 mW with neutral filters of various optical densities. The size of the laser beam at the sample was ~1.2 μm.

We used current-sensing atomic force microscopy (CSAFM) to test and image the electronic conductivity of individual grains of $LiNi_{0.8}Co_{0.15}Al_{0.05}O_2$ powder (Fuji Chemical) that was used to fabricate the composite cathodes. The powder was pressed

into a gold foil to produce randomly scattered particles of $LiNi_{0.8}Co_{0.15}Al_{0.05}O_2$ in good electronic contact with the Au substrate. The microscope consisted of a Molecular Imaging (MI) scanning probe microscope coupled with a Park Scientific Instruments (PSI) AutoProbe Electronic Module. The Si atomic force microscope (AFM) tips were coated with a thin conductive layer of W_2C. All CSAFM experiments were performed in constant-force mode with controlled oxide-tip voltage difference under a controlled dry N_2 atmosphere. A single scan of the tip over the sample surface simultaneously produced two images: a topographic image and a conductance image; the latter represents $Au/LiNi_{0.8}Co_{0.15}Al_{0.05}O_2$ - tip current variations during scanning at a given sample-tip voltage difference.

RESULTS

Figure 1 shows typical Raman microscopy spectra of a fresh composite $LiNi_{0.8}Co_{0.15}Al_{0.05}O_2$ cathode recorded at three different locations on the cathode surface. The Raman laser probe beam diameter was 1.2 µm, which is about one order of magnitude smaller that the size of an average $LiNi_{0.8}Co_{0.15}Al_{0.05}O_2$ particle (which is actually an agglomerate of smaller sub-micron crystallites). The Raman spectra of the fresh cathodes is dominated by two groups of bands: a broad maximum centered at ~510 cm^{-1}, characteristic for $LiNi_{0.8}Co_{0.15}Al_{0.05}O_2$ oxide, and two peaks at ~1350 and ~1600 cm^{-1}, which correspond to the D and G bands of elemental carbon, respectively. Recorded spectra of the fresh cathode vary as a function of location on the cathode surface, but carbon bands are predominant at almost all locations.

A semi-quantitative analysis of the cathode surface composition was carried out by deconvoluting Raman spectra into three electrode components. The three major bands at ~510, 1350, and 1580 cm^{-1} were integrated for each spectrum that was recorded at a given location on the cathode surface and expressed by red, blue, and green colors (trace [c] in Fig. 1). The saturation of each color is proportional to the integrated area under the respective Raman band for each location on the cathode surface. Thus, the resultant color corresponds to the local surface concentration of the $LiNi_{0.8}Co_{0.15}Al_{0.05}O_2$ active material (red), acetylene black (bright blue), and graphite (green), respectively. The two cathode carbon additives,

acetylene black and graphite, exhibit significant differences in their Raman signatures. Graphite (trace [b] in Fig. 1) exhibits a sharp and intense G-band at 1583 cm^{-1} and a weak D-band at 1345 cm^{-1}, which translate into predominantly green color signature from the band at 1583 cm^{-1}. In marked contrast to graphite, acetylene black (trace [a] in Fig. 1) displays broad, equally intense D and G Raman bands typical for disordered and amorphous-like carbons. Its spectral signature consists of nearly equal contributions from the D-band (blue) and G-band (green), which produce a light blue color. By recording individual spectra from various locations, cathode surface composition maps were produced with the Raman microscope. Thousands of Raman spectra were collected systematically from 52x75 μm sections of cathode surfaces at 0.7 μm resolution, deconvoluted, analyzed, and displayed as a color-coded points on the composition image map.

Representative micro-Raman surface composition image maps of a fresh cathode and the cathodes from high-power Li-ion cells that exhibited 10, 34, and 52% power loss are shown in Fig. 2. These unique composition maps clearly indicate that the fresh cathode surface is almost fully coated by acetylene black and graphite. Furthermore, the carbon coating is sufficiently thick to prevent detection of the underlying oxide active material. The cathode surface composition changed significantly in tested cells, which display much higher oxide/carbon surface concentration ratios. This composition change is particularly dramatic for the cathode from the cell with 52% power loss. This cathode surface consists almost entirely of bare oxide grains with only a few small regions of carbon additive. Although the color-coded maps represent a semi-quantitative comparison because of the different Raman scattering intensities of oxide and carbons, they clearly demonstrate dramatic changes in the electrode surface composition that accompanied cell tests. These data provide evidence for carbon retreat (or redistribution) from the cathode surface, a phenomenon that has escaped detection in prior diagnostic studies of Li-ion cells.

In order to determine if carbon redistribution or retreat also affects the bulk of the cathode, we carried out Raman micro-analysis of the cross-sections of $LiNi_{0.8}Co_{0.015}Al_{0.05}O_2$ cathode samples (Fig. 3). Samples of composite cathodes were prepared by folding the cathode until it cleaved and thereby exposed its cross-section.

Such a tool-less and non-invasive procedure allowed us **to reduce the risk of** sample contamination and possible structural damage. The results of the cross-section Raman microanalysis are consistent with our surface studies and clearly indicate that significant changes in the bulk (*i.e.*, sub-surface) $LiNi_{0.8}Co_{0.15}Al_{0.05}O_2$/elemental-carbon concentration ratio accompanied cell tests. We did not observe any clear carbon distribution pattern across the electrode thickness. **This absence of a distribution pattern may be a result of the sample preparation, which could possibly alter the distribution of the cathode components**. However, the extent of carbon retreat observed in the cathode bulk was somewhat smaller than that on the cathode surface.

We looked for carbon residue in DMC, which was used to wash the cathodes to determine if washing/rinsing could lead to carbon removal from the electrode surface. Indeed, we found a small amount of carbon precipitate present in each solvent sample. Its amount varied slightly but it did not follow the trend observed in our Raman surface analysis. In fact, we found more carbon in DMC used to wash the fresh sample than in the post-wash DMC solutions of tested cathodes.

Figure 4 shows CSAFM images of surface conductance (right-hand panel) and topography (left-hand panel) of a representative 5 x 5 μm region of the composite $LiNi_{0.8}Co_{0.15}Al_{0.05}O_2$ cathode surface at 1.0 V tip-sample voltage difference from (A) a fresh cell; and (B) a cathode from the cell, which lost 34% of its power. The surface morphology images of both cathodes (left-hand panel) show large polycrystalline agglomerates and reveal no significant changes in the cathode surface topography in tested cells. This result is contrary to our earlier study of the $LiNi_{0.8}Co_{0.2}O_2$ cathodes, which showed that considerable amounts of nanocrystalline deposits accumulated in the cathode inter-granular spaces and across the crystal planes [2,3].

The conductance images in the right-hand panel of Fig. 4 show both dark and white regions, which correspond to local areas of high and low (or zero) electronic conductance, respectively. The surface conductance image of the cathode from a fresh cell exhibits areas of mostly high electronic conductance and only a few insulating regions. Highly conductive graphite and acetylene black additives, which are abundant in

the composite cathode, constitute a conductive matrix in the cathode surface and bulk, and are primarily responsible for the excellent electronic properties observed at the cathode surface. The $LiNi_{0.8}Co_{0.15}Al_{0.05}O_2$ may also contribute to the tip current, but its contribution is substantially lower than that of carbon. The insulating areas on the cathode surface are most likely associated with the presence of PVDF binder, solid electrolyte interphase (SEI) products, and unusual surface morphology (*e.g.*, deep crevices).

The conductance images of cathodes tested at elevated temperatures show a dramatic increase of surface resistance. Most of the cathode surface became insulating except for a few locations, mainly in deep crevices and intergranular spaces, which remained conductive. Previous results for $LiNi_{0.8}Co_{0.2}O_2$ cathodes [2,3] also showed a complete lack of conductivity of the cathode surface, consistent with either loss of contact of particles at the electrode surface with the rest of the electrode, or the presence of a non-conductive film of polycarbonates, and LiF, Li_xPF_y-type and $Li_xPF_yO_z$-type compounds [13].

A reduction in conductance of portions of the cathode can easily explain the observed increase in cell impedance as well as loss of cathode capacity *via* isolation of oxide active material. Particle isolation is also in concert with our observations of carbon retreat or rearrangement in tested cathodes. These results represent the most clear and obvious difference (compared to other diagnostic studies) in cathode characteristics after prolonged cell tests at elevated temperatures. However, the intrinsic conductivity of the $LiNi_{0.8}Co_{0.15}Al_{0.05}O_2$ (10^{-2}-10^{-3} S cm^{-1}) should be sufficiently high to compensate for a partial carbon loss or carbon rearrangement within the thin (40 μm) cathode bulk. In other words, the potential drop across a 40 μm pure (*i.e.*, with no carbon additive) $LiNi_{0.8}Co_{0.15}Al_{0.05}O_2$ cathode cannot account for the observed cell power loss, not to mention the irreversible capacity loss that always accompanies the cathode impedance increase.

In order to better understand the potential role of carbon retreat/redistribution on cathode impedance rise and capacity loss we designed a new diagnostic test to investigate the intrinsic electronic properties of $LiNi_{0.8}Co_{0.15}Al_{0.05}O_2$ particles. Individual 10-20 μm agglomerates of $LiNi_{0.8}Co_{0.15}Al_{0.05}O_2$ were pressed into a gold foil,

and then their local electronic properties were investigated *via* CSAFM. The surfaces of these embedded particles were scanned with a conductive AFM tip with a potential of 1V applied between the sample and the tip. The morphology image and the corresponding surface conductance map are shown in Fig. 5. Large agglomerates of $LiNi_{0.8}Co_{0.15}Al_{0.05}O_2$ consist of smaller (sub-micron to ~5 microns) crystallites fused tightly together. The conductance image revealed that the agglomerate crystallites were not uniformly conductive. Surprisingly, some crystallites displayed good electronic contact with the Au substrate (as expected) and some exhibited very high resistance, representing the lack of a facile electronic pathway to the Au substrate. We attribute this non-uniformity in electronic properties to poor inter-crystallite (*i.e.*, inter-granular) electronic contact. This poor contact inhibits electrons from reaching crystallites that are not in direct contact with the Au current collector. The presence of a nascent thin insulating surface region of Li_xNiO [1], a resistive film (Li_2CO_3) coating some of the $LiNi_{0.8}Co_{0.15}Al_{0.05}O_2$ crystallites, or poor mechanical contact between crystallites may be responsible for the observed effect.

We propose the following power and capacity fade scenario for Li-ion composite cathodes based on our diagnostic results. The presence of a relatively large amount of carbon additives uniformly distributed in the fresh composite $LiNi_{0.8}Co_{0.15}Al_{0.05}O_2$ cathode provides a conductive path not only between large agglomerates and the Al current collector but also between crystallites within the agglomerates. The excess of carbon neutralizes the inherently poor nascent inter-granular electronic contact because it provides an additional connection path to the current collector through the carbon matrix. The observed carbon retreat (or possibly carbon redistribution) at the cathode surfaces of tested cells can "expose" small crystallites within agglomerates. If these particles were originally in poor electronic contact with their neighbors, then the consequent loss of a direct electronic path through the receding carbon matrix will lead to an increased resistance within the agglomerate and, eventually, total isolation of some particles. **It is also possible that the intergranular electronic contact within agglomerates could deteriorate even further during cell cycling/ageing due to a mechanical stress, thin film formation, gas evolution etc.** Thus, we postulate that the combination of carbon retreat (or rearrangement) and the intrinsic electronic properties of the

$LiNi_{0.8}Co_{0.15}Al_{0.05}O_2$ powder is responsible for the observed cell power and capacity fade. A simple circuit model of such a scenario, based on a distributed network, confirmed that such a superposition of effects can lead to a significant shift of the low-frequency intercept in the impedance spectra with a minimal effect on the position of the high-frequency intercept, as is observed [1].

.Further fundamental studies of the specific phenomena that cause carbon retreat or redistribution at the surface of lithium-ion battery cathodes are underway. **Among possible scenarios we consider: (i) loss of adhesion to the cathode surface, (ii) mechanical rearrangement/agglomeration , (iii) gas evolution, (iv) SEI layer formation, (v) carbon oxidation, (vi) electrophoretic transport of carbon toward the anode, (vii) alteration of the Raman scattering cross-section of the carbon e.g., anion intercalation into carbon.**

REFERENCES

1. FY 2002 Progress Report for Energy Storage Research and Development, which can be downloaded from the U.S. Department of Energy web site at http://www.eere.energy.gov/vehiclesandfuels/resources/fcvt_publications.shtml

2. X. Zhang, P. N. Ross, Jr., R. Kostecki, F. Kong, S. Sloop, J. B. Kerr, K. Striebel, E. J. Cairns and F. McLarnon, *J. Electrochem. Soc.*, 148 (2001) 463.

3. R. Kostecki and F. McLarnon, *Electrochem. Solid State Lett.,* **5***,* A164 (2002).

4. D. P. Abraham, R. D. Twesten, M. Balasubramanian, J. Kropf, D. Fischer, J. McBreen, I. Petrov, K. Amine, *J. Electrochem. Soc.***, 150**, A1450 (2003).

5. I. Rey, J.C. Lassègues, P. Baudry, H. Majastre, Electrochim. Acta, **43**, 1539 (1998).

6. J.-C. Panitz, F. Joho, P. Novák, Appl. Spectrosc., **53**, 1188 (1999).

7. P. Novák, J.-C. Panitz, F. Joho, M. Lanz, R. Imhof, M. Coluccia, J. Power Sources, 90, 52 (2000).

8. J.-C. Panitz, P. Novák, J. Power Sources, **97-98**, 174 (2001).

9. J.-C. Panitz, P. Novák, O. Haas, Appl. Spectrosc., **55**, 1131 (2001).

10. Y. Luo, W.-B. Cai, D.A. Scherson, Electrochem. Solid-State Lett., **4**, A101 (2001).

11. Y. Luo, W.-B. Cai, D.A. Scherson, J. Electrochem. Soc., **149**, A1100 (2002).

12. R. Kostecki, F. McLarnon, J. Power Sources, **119-121**, 550 (2003).

13. A. M. Andersson, D. P. Abraham, R. Haasch, S. MacLaren, J. Liu, and K. Amine, *J. Electrochem. Soc.*, **149**, A1358 (2002)
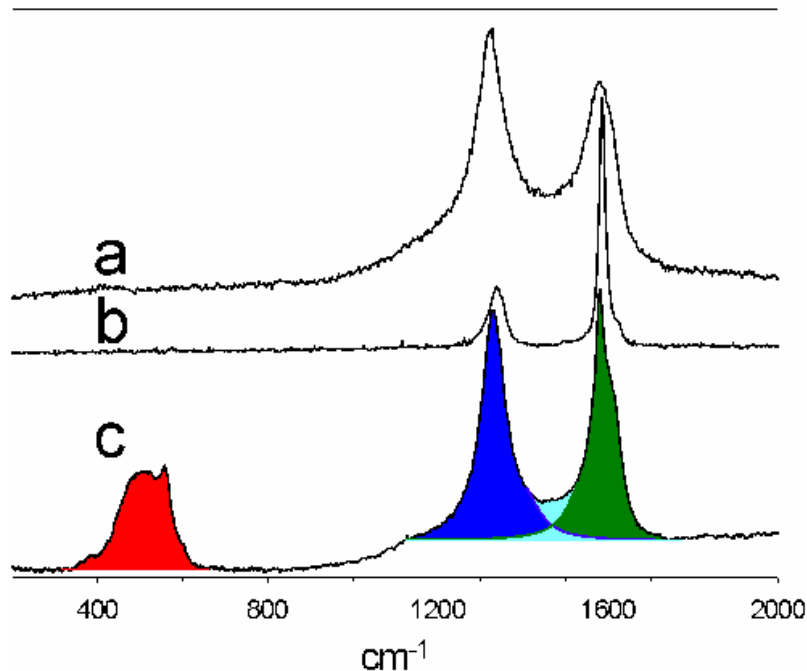
Figure 1. Typical Raman microscope spectra of the fresh composite $LiNi_{0.8}Co_{0.15}Al_{0.05}O_2$ cathode recorded at different surface locations. Spectra (a), (b), and (c) correspond to surface regions dominated by disordered carbon, graphitic carbon, and oxide, respectively. The color-coding analysis scheme is illustrated by spectrum (c).
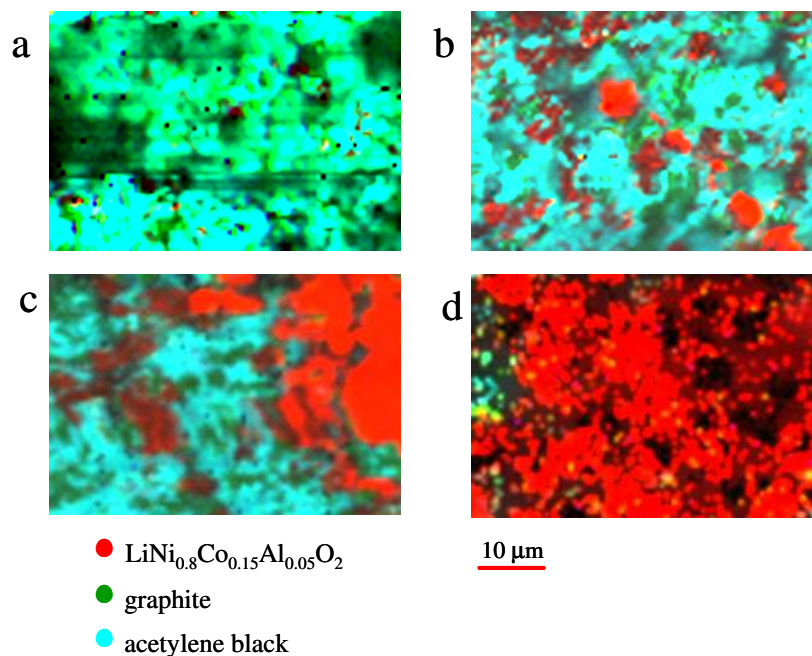

● $LiNi_{0.8}Co_{0.15}Al_{0.05}O_2$

● graphite

● acetylene black

10 μm

Figure 2. 52 x 75 μm Raman microscope images of the composite $LiNi_{0.8}Co_{0.15}Al_{0.05}O_2$ cathodes. The images consist of Raman spectra collected at 0.7 μm resolution. The intensity of red, blue and green color corresponds to the integrated bands intensity of $LiNi_{0.8}Co_{0.15}Al_{0.05}O_2$, and D, G carbon bands of each spectrum, respectively. (a) fresh cathode, (b), (c) and (d) cathodes from cells which lost 10, 34, and 52% of power, respectively.
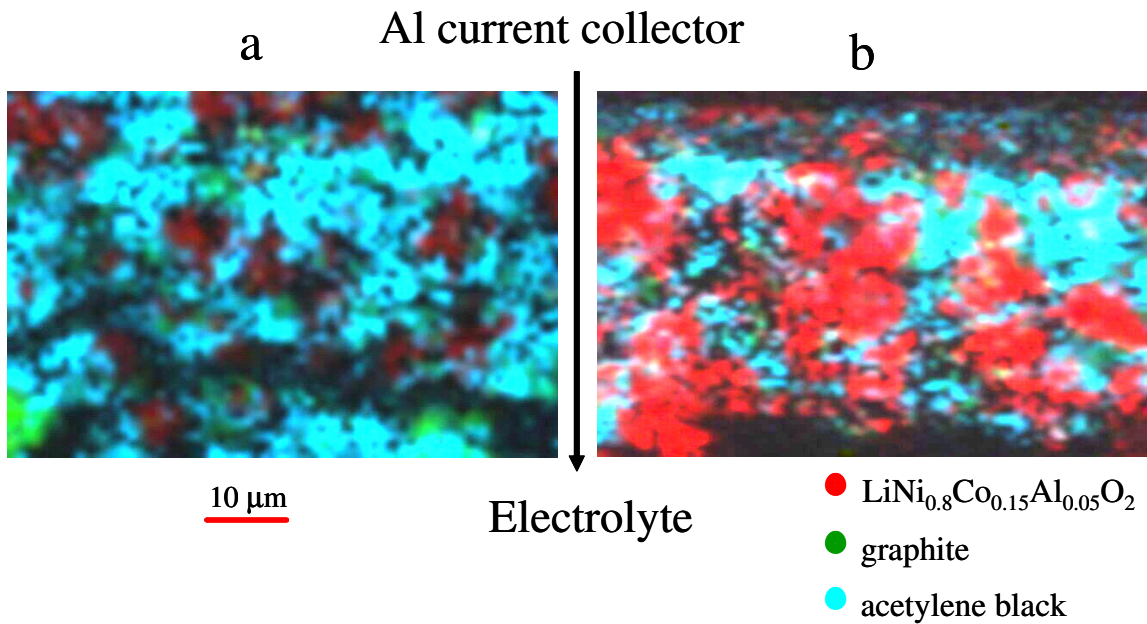
a

Al current collector

b

10 μm

Electrolyte

● $LiNi_{0.8}Co_{0.15}Al_{0.05}O_2$

● graphite

● acetylene black

Figure 3. 52 x 75 μm Raman microscope images of a cross-section of the composite $LiNi_{0.8}Co_{0.15}Al_{0.05}O_2$ cathodes. (a) fresh cathode, (b)cathode from the cells which lost 52% of power.
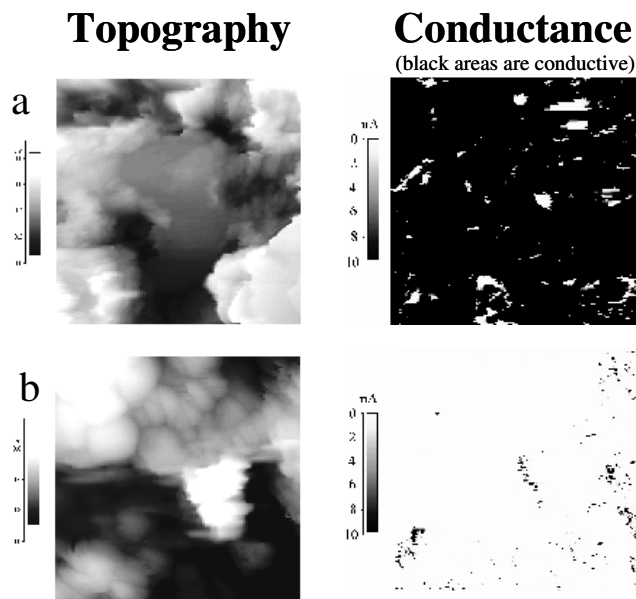

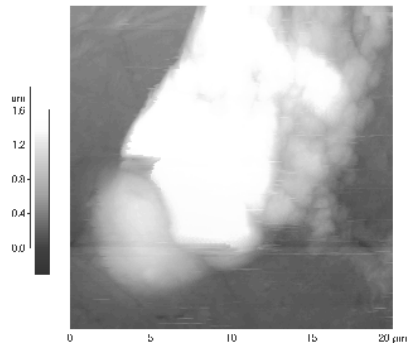**Topography**   **Conductance**
(black areas are conductive)

a

b

Figure 4. CSAFM images of surface conductance (right-hand panel) and topography (left-hand panel) of a 5 x 5 μm region of the composite $LiNi_{0.8}Co_{0.15}Al_{0.05}O_2$ cathode surface at 1.0 V tip-sample voltage difference: (A) virgin cell; (B) cathode from the cell which lost 34% of power.

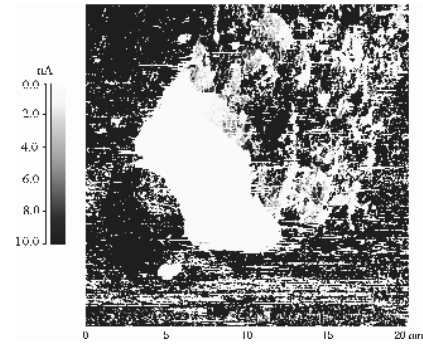**Topography**   **Conductance**

(black areas are conductive)

Figure 5. 20 x 20 μm CSAFM images of surface conductance and topography of a single particle of $LiNi_{0.8}Co_{0.15}Al_{0.05}O_2$ embedded into a Au foil at 1.0 V tip-sample voltage difference.